Enabling visible-light absorption and p-type doping in In$_2$O$_3$ by adding Bi

Fernando P. Sabino,[1,*] Su-Huai Wei,[2,†] and Anderson Janotti[1,‡]

[1]*Department of Materials Science and Engineering, University of Delaware, Newark, Delaware 19716, USA*
[2]*Beijing Computational Science Research Center, Beijing 100094, China*

In$_2$O$_3$ is a prototype wide-band-gap semiconductor that exhibits metallic conductivity when highly doped with Sn whereas retaining a high degree of transparency to visible light. It is widely used as a transparent window/electrode in solar cells and light-emitting diodes. The functionality of In$_2$O$_3$ would be greatly extended if p-type conductivity could also be achieved. Using electronic structure calculations, we show that adding Bi to In$_2$O$_3$ in the form of dilute (In$_{1-x}$Bi$_x$)$_2$O$_3$ alloys leads to a new valence band that is sufficiently higher in energy than the original O $2p$ valence band to allow for p-type doping. Moreover, the raised valence band in the (In$_{1-x}$Bi$_x$)$_2$O$_3$ dilute alloys leads to strong optical absorption in the visible spectrum, opening up for new applications, such as a wide-band-gap absorber layer in tandem solar cells.

I. INTRODUCTION

In$_2$O$_3$ is a wide-band-gap material, extensively used as a transparent conducting oxide. When heavily doped with Sn, often called indium tin oxide (ITO), it displays electrical conductivities around 1×10^3 S/cm, whereas preserving a high transparency to visible light [1,2]. The combination of optical transparency and high electrical conductivity is desirable for many device applications, such as liquid-crystal displays, organic light-emitting diodes, touchscreens, and transparent contacts in photovoltaic devices [3–6]. The functionality of In$_2$O$_3$ would be greatly expanded if p-type conductivity could also be achieved [7,8].

Most common dopants in In$_2$O$_3$ act as donors, including hydrogen [9,10]. This is explained by the relatively low position of the conduction band with respect to the vacuum level. A major difficulty in making an In$_2$O$_3$ p-type is related to fundamental characteristics of its valence band [1,11]. It is composed of O $2p$ orbitals and lies very low in energy with respect to the vacuum level so that all possible acceptor impurities lead to deep levels in the gap with very high ionization energies [12]. Attempts to modify the electronic structure of wide-gap oxides to enable p-type doping have been proposed yet with limited success [8,13]. The key strategy has been to modify the top of the valence band by enhancing covalence through orbital hybridization between O $2p$ and metal cations [8,13] or by incorporating isovalent anions, such as S and Se, with valence p orbitals that are higher in energy and more delocalized than the O $2p$ [14,15]. Building on recent ideas of using compounds containing post-transition metals to modify the valence band [16–18], here we explore adding low concentrations of Bi to In$_2$O$_3$. We report on the stability as well as the electronic structure and optical properties of (In$_{1-x}$Bi$_x$)$_2$O$_3$ dilute alloys.

Bismuth belongs to the column 5A of the periodic table. In III–V semiconductors, such as GaAs, InAs, and InSb, Bi substitutes on the pnictide sites, acting as an isovalent pentavalent addition. However, Bi is also known to behave as a trivalent species, such as in Bi$_2$Se$_3$ [19] and Bi$_2$O$_3$ [20,21]. Considering the atomic size difference between In and O in In$_2$O$_3$, we expect that Bi will substitute on the In site.

Using density functional theory with a hybrid functional we calculate the electronic structure of dilute (In$_{1-x}$Bi$_x$)$_2$O$_3$ alloys with $x = 0.78\%$, 3.13%, 6.25%, and 12.5% . We find that Bi leads to an occupied band, composed of Bi s and O p orbitals, that is significantly higher in energy than the valence-band maximum (VBM) of the host material In$_2$O$_3$. The band gap as well as the position and bandwidth of this new valence band can be tuned with Bi concentration. Furthermore, this raised valence band in (In$_{1-x}$Bi$_x$)$_2$O$_3$ dilute alloys not only leads to strong optical absorption in the visible spectral region, but also potentially enables p-type doping.

II. COMPUTATIONAL APPROACH

Our first-principles calculations are based on the density functional theory [22,23] and the hybrid functional of Heyd-Scuseria-Ernzerhof (HSE06) [24,25] as implemented in the VASP code [26,27]. For the interaction between the valence electrons and the ionic cores, we used augmented plane-wave potentials [28,29] with the following valence configurations: O($2s^2 2p^4$), In($4d^{10} 5s^2 5p^1$), and Bi($5d^{10} 6s^2 6p^3$). The volume and atomic positions were relaxed using the semilocal exchange and correlation functional of Perdew, Burke, and Ernzerhof (PBE) parametrized for solids (PBESol) [30] with an energy cutoff of 620 eV for the plane-wave expansion. For integrations over the Brillouin zone, we employed a $3 \times 3 \times 3$ **k**-point mesh for the 40-atom primitive cell of bixbyite In$_2$O$_3$ and the same **k**-point density for the other supercells.

Since PBE or PBESol drastically underestimate band gaps [24,25,31], we use the HSE06 to calculate the electronic structure of In$_2$O$_3$ and (In$_{1-x}$Bi$_x$)$_2$O$_3$ alloys. The HSE06

———————
*fernandopsabino@yahoo.com.br
†suhuaiwei@csrc.ac.cn
‡janotti@udel.edu

calculations were carried out for the crystal structures optimized with PBESol. In HSE06, the nonlocal Fock exchange is separated in short- and long-range parts by a screening function determined by the parameter $\omega = 0.206 \, \text{Å}^{-1}$ [24,25]. In the short-range region we used 25% of the exact exchange and 75% of the PBE exchange, whereas the long-range part is described by the PBE exchange [24,25]. The electronic band structure and density of states were computed with a lower cutoff energy of 470 eV and a large $7 \times 7 \times 7$ **k**-point mesh. For the optical properties we use the tetrahedral smearing method but do not include excitonic effects due to the prohibitive computational cost.

III. RESULTS AND DISCUSSION

A. Structural and electronic properties

In_2O_3 crystallizes in the body-centered-cubic bixbyite structure [32] with space-group $Ia\overline{3}$ and having 40 atoms (8 formula units) in the primitive cell. All the O sites are equivalent, and each O atom is bonded to four In atoms, whereas each In atom is bonded to six O atoms. There are two inequivalent In octahedral sites, one forming a distorted octahedron ($24d$), and the other forming a perfect octahedron ($8b$) with all In-O bonds equal in length. Therefore, there are two possible sites for Bi to substitute on In in the bixbyite structure. We tested Bi substitution on both sites, and we find that Bi occupying the perfect octahedral site is only 12 meV lower in energy than the distorted site for $(In_{1-x}Bi_x)_2O_3$ with $x = 1/16$ (6.25%). The difference in the electronic structure of these two configurations is negligible with band gaps differing by less than 10 meV. Therefore, we expect that Bi will incorporate on both perfect and distorted octahedral sites during growth. We also tested In incorporating on the O site and found that would lead to a much higher-energy configuration, independent of the oxygen chemical potential and Fermi-level position.

$(In_{1-x}Bi_x)_2O_3$ alloy structures used in the simulations were built as follows: We used the 40-atom primitive cell with one Bi replacing one In for $x = 1/16 = 6.25\%$; the conventional 80-atom unit cell with one Bi replacing one In to describe the alloy $x = 1/32 = 3.125\%$, and a 320-atom supercell ($2 \times 2 \times 2$ repetition of the primitive cell) with one Bi replacing one In to represent the alloy with $x = 1/128 = 0.78\%$. The alloy concentration $x = 1/8 = 12.5\%$ was simulated using a special quasirandom structure (SQS) [33,34] based on the 80-atom conventional unit cell where four Bi replace four In atoms.

The calculated lattice parameter a_0 and volume per formula unit of In_2O_3 and $(In_{1-x}Bi_x)_2O_3$ alloys are listed in Table I. The calculated lattice parameter of 10.14 Å for In_2O_3, using PBESol, is only 0.2% larger than the experimental value of 10.12 Å [32]. Adding Bi to In_2O_3 leads to an increase in the lattice parameter since Bi has a larger atomic radius than In. We also calculated the mixing enthalpy for the $(In_{1-x}Bi_x)_2O_3$ alloys, which we define as

$$\Delta H^f = E_{\text{tot}}[(In_{1-x}Bi_x)_2O_3] - (1-x)E_{\text{tot}}(In_2O_3) \\ - xE_{\text{tot}}(Bi_2O_3), \quad (1)$$

TABLE I. Calculated lattice parameter a, volume, and mixing enthalpy (ΔH^f) per cation of $(In_{1-x}Bi_x)_2O_3$ alloys for various Bi concentrations (x). For comparison, the experimental equilibrium lattice parameter of In_2O_3 and volume per formula unit are 10.12 Å and 64.78 Å^3 [32].

System	x (%)	Lattice parameter a_0 (Å)	Volume (Å^3/f.u.)	ΔH^f (meV/cation)
In_2O_3	0	10.14	65.15	0
$(In_{1-x}Bi_x)_2O_3$	0.78	10.15	65.33	2
$(In_{1-x}Bi_x)_2O_3$	3.13	10.17	65.74	13
$(In_{1-x}Bi_x)_2O_3$	6.25	10.20	66.33	25
$(In_{1-x}Bi_x)_2O_3$	12.5	10.26	67.49	52

where $E_{\text{tot}}[(In_{1-x}Bi_x)_2O_3]$ is the total energy of the alloy, $E_{\text{tot}}(In_2O_3)$ is the total energy of In_2O_3, and $E_{\text{tot}}(Bi_2O_3)$ is the total energy of Bi_2O_3 in its ground state. The calculated formation enthalpy of the $(In_{1-x}Bi_x)_2O_3$ alloys are comparable to that found in $(Ga_{1-x}In_x)_2O_3$ [35], which have been demonstrated experimentally [36]. For instance, $\Delta H^f = 52$ meV/cation for $(In_{1-x}Bi_x)_2O_3$ with $x = 12.5\%$, whereas $\Delta H^f = 50$ meV/cation for $(Ga_{1-x}In_x)_2O_3$ for the same x [35]. Therefore, these relatively low values of mixing enthalpies indicate that $(In_{1-x}Bi_x)_2O_3$ alloys are likely to form.

The calculated electronic band structure of In_2O_3 and $(In_{1-x}Bi_x)_2O_3$ alloy with $x = 1/16$, their density of states (DOS) and the DOS with Bi concentration of $x = 1/8$ are shown in Fig. 1. Note that for $x = 1/16$ an "ordered" structure was used to model the $(In_{1-x}Bi_x)_2O_3$ alloy which maximize the Bi-Bi distance. In practice, we expect that random distribution of Bi would lead to a broadening of the band. Thus for $x = 1/8$, which Bi occupation was determined by SQS, we plot only the DOS.

The band structure and the DOS for In_2O_3, calculated using HSE06, shows a fundamental band gap of 2.63 eV, which is slightly lower than the previously reported value of 2.80 eV [1]. Adding Bi leads to a fully occupied band which is significantly higher in energy than the original VBM of the host In_2O_3 material. This band originates from the coupling between the Bi s state, which is well below the VBM, with O $2p$ states, mainly from the O atoms next to the Bi. Therefore, it has an antibonding character from the Bi s O p coupling. The minimum occurs at Γ and the maximum (VBM) occurs at the H point for the ordered alloy at $x = 1/16$. Note that, in a random alloy as it is modeled for $(In_{1-x}Bi_x)_2O_3$ with $x = 1/8$, the plot of the density of states as shown in Fig. 1(c) is more relevant.

For the $(In_{1-x}Bi_x)_2O_3$ alloy with $x = 1/16$, we find a band gap of 2.01 eV with a new VBM about 1.28 eV higher than the VBM of In_2O_3. The bandwidth of this higher valence band is 0.52 eV. The conduction-band minimum (CBM) of the alloy at Γ is also pushed up by 0.66 eV, largely due to the interaction with the Bi s band. When the Bi concentration increase to $x = 1/8$, the band gap increased to 2.29 eV with the antibonding Bi s bandwidth of 1.00 eV, and the CBM is pushed up by 1.03 eV.

The evolution of the band structure of the dilute $(In_{1-x}Bi_x)_2O_3$ alloy with Bi concentration with respect to that of the parent compound In_2O_3 is shown in Fig. 2. The

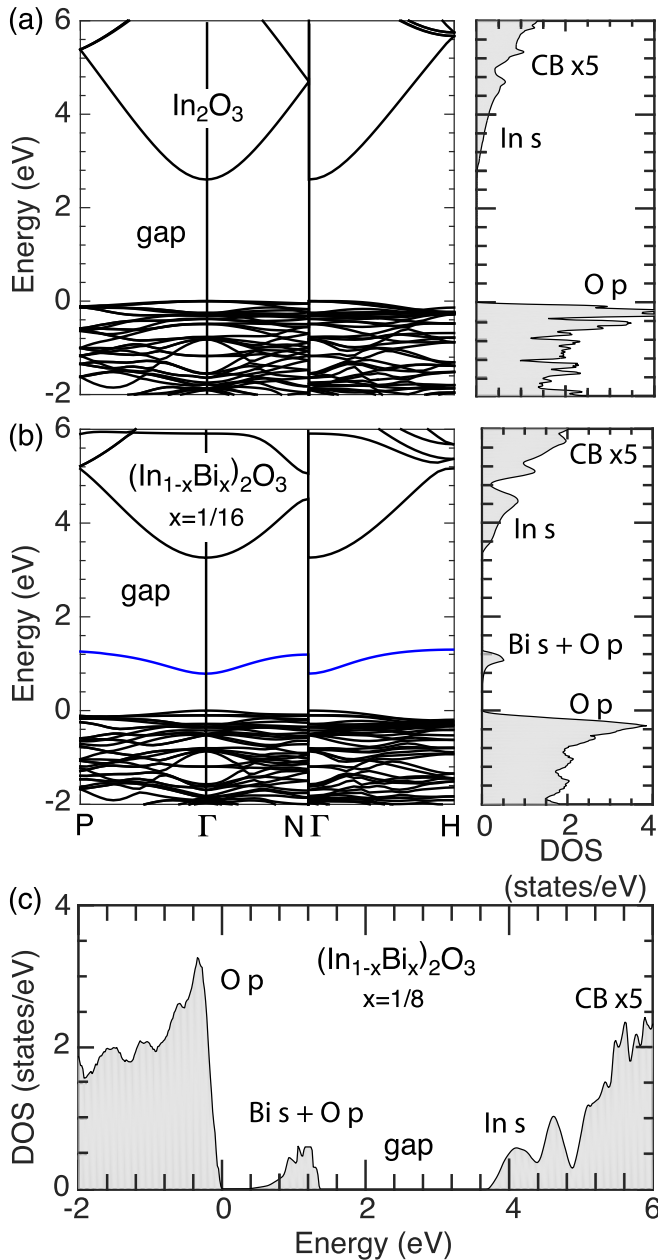FIG. 1. Calculated band structure and density of states for (a) In_2O_3 and (b) $(In_{1-x}Bi_x)_2O_3$ with $x = 1/16$ both in the primitive cell of bixbyite structure. Also, the density of state for (c) $(In_{1-x}Bi_x)_2O_3$ with $x = 1/8$ in the conventional structure was calculated. For all the systems, we aligned the bands using the averaged electrostatic potential over an In atom in the bulk In_2O_3 and in an In atom far from Bi in the $(In_{1-x}Bi_x)_2O_3$ alloy. The VBM of In_2O_3 was used as reference, and it indicates that the VBM of the alloy is 1.28 eV ($x = 1/16$) and 1.37 eV ($x = 1/8$) higher than the original VBM of the host material.

maximum of the O $2p$ band in the $(In_{1-x}Bi_x)_2O_3$ alloy occurs at approximately the same energy position as the VBM of the host In_2O_3, which is composed of O $2p$. Our results indicate that we can tune three key parameters in the $(In_{1-x}Bi_x)_2O_3$ alloy by changing the Bi concentration: The positions of the valence-band (now derived from the antibonding Bi s state)

and conduction-band edges, the bandwidth of the valence band, and the band gap.

The repulsion between the Bi s valence band and the lowest-energy conduction band also plays an important role in determining the band gap of the alloy. Although the fundamental gap is direct at Γ in In_2O_3, it becomes indirect in the (ordered) alloy with the VBM at the H point for $x = 1/16$ and $1/128$ and at the R point for $x = 1/32$. For the random alloys $x = 1/8$, the band gap has a pseudodirect nature.

B. Optical properties

We also calculated the absorption coefficient of dilute $(In_{1-x}Bi_x)_2O_3$ alloys. Due to the high computational cost of calculating the optical properties of large systems with sufficient number of **k** points in HSE06, we performed these calculations using PBESol and then applied a scissors operator to correct the fundamental band gap according to the HSE06 results. This approximation does not affect the lowest-energy optical transitions as tested using HSE06 and PBESol for $(In_{1-x}Bi_x)_2O_3$ with $x = 1/16$.

The optical properties of In_2O_3 are well described in the literature, including the disparity between the optical and fundamental band gap [1,11,37,38]. It has been now accepted that the disparity between the optical and the fundamental band gap is attributed largely to forbidden or weakly allowed transitions from the upper most valence bands and the conduction band with some contribution from the Burstein-Moss shift due to the presence of electrons in the conduction band [1,11,38]. As shown in Fig. 3(a), our results reproduce previous calculations for In_2O_3 where the optical absorption starts to increase only at photon energies that are 0.8 eV larger than the fundamental band-gap E_g^F, defining the optical band-gap E_g^O. Optical transitions with energy in the range from E_g^F to E_g^O have negligible contributions to the optical absorption coefficient with magnitude smaller than 1×10^{-4} as indicated in Fig. 3. This small contribution comes from the weak transitions from valence-band to conduction-band states at or in the vicinity of the Γ point [39].

As shown in Figs. 3(b)–3(d), we see a redshift in the onset of absorption of $(In_{1-x}Bi_x)_2O_3$ alloys. This redshift decreases as the Bi concentration increases, consistent with the variation of the band gap with Bi concentration shown in Figs. 2 and 1. The peak associated with the transition from the antibonding Bi s valence band to the conduction band increases with the Bi concentration. We note, however, a seeming disparity between the optical and the fundamental band gap in the $(In_{1-x}Bi_x)_2O_3$ alloys as shown in Figs. 3(b)–3(d). The origin of this disparity is associated to the indirect band gap in the alloys simulated using periodic supercells and forbidden or very weak transition from the hybridized Bi s band to CBM. In a real random alloy, the lack of long-range order would lead to the collapse of the Brillouin zone to the Γ point, and the discussion of direct versus indirect band gap will lack meaning so that we would expect transitions near or at the fundamental band gap to be allowed but perhaps weak.

We note that the VBM in the $(In_{1-x}Bi_x)_2O_3$ alloys is sufficiently higher in energy than the VBM in In_2O_3 to allow for p-type doping. For example, introducing Mg dopants in

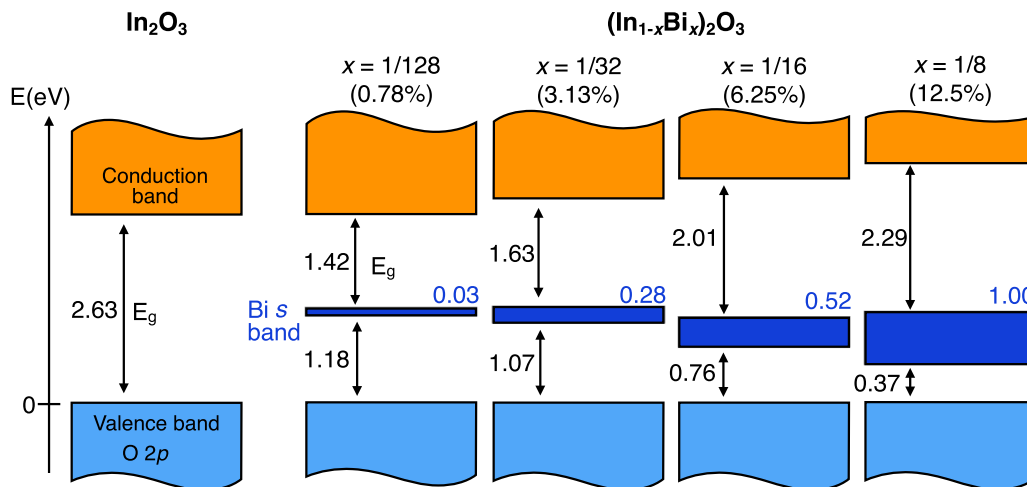FIG. 2. Position of the valence and conduction bands in In_2O_3 and dilute $(In_{1-x}Bi_x)_2O_3$ alloys for Bi concentrations of $x = 1/128$ (0.78%), 1/32 (3.13%), 1/16 (6.25%), and 1/8 (12.5%). We used the VBM of In_2O_3 as reference and aligned the band edges of the alloys as described in the text. Bi leads to a fully occupied band which is significantly higher in energy than the original VBM of the host In_2O_3 material. This band originates from the coupling between the Bi s state with O $2p$ states. Furthermore, the band gap of In_2O_3 and $(In_{1-x}Bi_x)_2O_3$ alloys as well as the bandwidth of the hybrid O p and Bi s bands (valence bands in the alloys), and the distance to the O $2p$ bands are indicated.

In_2O_3 leads to a deep acceptor level in the gap associated with the hole localized on an O atom next to the Mg_{In} substitutional impurity [12]. This acceptor level is about 0.9 eV above the VBM in In_2O_3. Therefore, in dilute $(In_{1-x}Bi_x)_2O_3$ alloys, the same acceptor level is expected to appear close to the

FIG. 3. Calculated absorption coefficient as a function of photon energy for In_2O_3 and $(In_{1-x}Bi_x)_2O_3$ with Bi concentrations $x = 1/8$, $x = 1/16$, and $x = 1/32$. The vertical dashed lines indicate the fundamental band gap (E_g^F) and the optical band gap (E_g^O). The disparity between E_g^F and E_g^O is also indicated.

antibonding Bi-s-derived VBM in the alloy (see band alignment in Fig. 2), making it a shallow acceptor.

Finally, we believe our results can explain some puzzling results on In_2O_3 samples containing Bi. A high intensity emission peak at 1.8 eV in the spectrum of nanocomposites of Bi-doped ITO has been reported by Na *et al.* [40]. The authors have attributed this emission to a transition from the conduction band to deep levels related to O vacancies. However, based on our results, for Bi concentration of approximately 1% in their experiments, the predicted optical band gap of the dilute $(In_{1-x}Bi_x)_2O_3$ alloy is 1.8 eV, and a transition from the conduction band to the antibonding Bi s band can explain this emission peak.

Considering the strong optical absorption in the visible spectrum of dilute $(In_{1-x}Bi_x)_2O_3$ alloy, the conduction-band offset with In_2O_3, and the possibility of doping it p type, we can think of $(In_{1-x}Bi_x)_2O_3$ as a wide-band-gap absorption layer to be integrated in tandem solar cells where ITO is used as transparent contact. Note that there will be a trade-off between the band gap and the width of the antibonding Bi s valence band, which will have to be taken into consideration in the device design.

IV. SUMMARY

To summarize, using electronic structure calculations, we show that incorporating low concentrations of Bi into In_2O_3, forming dilute $(In_{1-x}Bi_x)_2O_3$ alloys, leads to significant changes in the electronic and optical properties of the parent compound, greatly extending its functionality. The Bi introduces an occupied intermediate valence band, composed mainly of Bi s and O p, resulting in significantly reduced band gaps. The position and bandwidth of the new valence band in the $(In_{1-x}Bi_x)_2O_3$ alloys can be tuned by controlling the Bi concentration. The high VBM of the $(In_{1-x}Bi_x)_2O_3$ alloys can possibly enable p-type doping. The reduced band gap, compared to In_2O_3 and strong near-band-edge absorption make
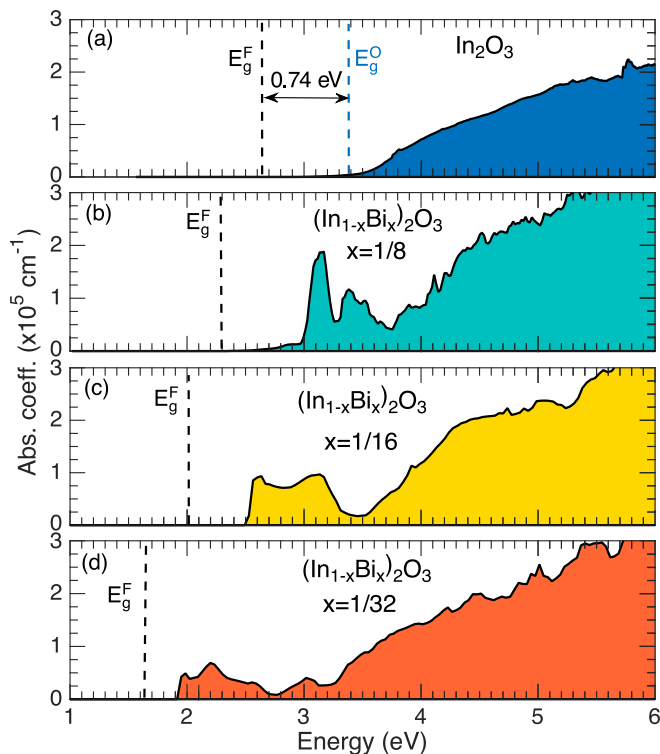
dilute $(In_{1-x}Bi_x)_2O_3$ alloys a promising wide-gap absorber layer in tandem solar cells.

[1] A. Walsh, J. L. F. Da Silva, S.-H. Wei, C. Körber, A. Klein, L. F. J. Piper, A. DeMasi, K. E. Smith, G. Panaccione, P. Torelli, D. J. Payne, A. Bourlange, and R. G. Egdell, Phys. Rev. Lett. **100**, 167402 (2008).

[2] Z. Chen, W. Li, R. Li, Y. Zhang, G. Xu, and H. Cheng, Langmuir **29**, 13836 (2013).

[3] K. Nomura, H. Ohta, K. Ueda, T. Kamiya, M. Hirano, and H. Hosono, Science **300**, 1269 (2003).

[4] K. Nomura, H. Ohta, A. Takagi, T. Kamiya, M. Hirano, and H. Hosono, Nature (London) **432**, 488 (2004).

[5] T. Minami, Semicond. Sci. Technol. **20**, S35 (2005).

[6] C. G. Granqvist, Sol. Energy Mater. Sol. Cells **91**, 1529 (2007).

[7] Y. Xu and M. A. Schoonen, Am. Mineral. **85**, 543 (2000).

[8] K. H. L. Zhang, K. Xi, M. G. Blamire, and R. G. Egdell, J. Phys.: Condens. Matter **28**, 383002 (2016).

[9] T. Koida, H. Fujiwara, and M. Kondo, Jpn. J. Appl. Phys., Part 2 **46**, L685 (2007).

[10] T. Koida, M. Kondo, K. Tsutsumi, A. Sakaguchi, M. Suzuki, and H. Fujiwara, J. Appl. Phys. **107**, 033514 (2010).

[11] F. P. Sabino, R. Besse, L. N. Oliveira, S.-H. Wei, and J. L. F. Da Silva, Phys. Rev. B **92**, 205308 (2015).

[12] S. Lany and A. Zunger, Phys. Rev. B **80**, 085202 (2009).

[13] H. Kawazoe, M. Yasukawa, H. Hyodo, M. Kurita, H. Yanagi, and H. Hosono, Nature (London) **389**, 939 (1997).

[14] H. Hiramatsu, K. Ueda, H. Ohta, M. Orita, M. Hirano, and H. Hosono, Thin Solid Films **411**, 125 (2002).

[15] H. Hiramatsu, K. Ueda, H. Ohta, M. Hirano, M. Kikuchi, H. Yanagi, T. Kamiya, and H. Hosono, Appl. Phys. Lett. **91**, 012104 (2007).

[16] Y. Ogo, H. Hiramatsu, K. Nomura, H. Yanagi, T. Kamiya, M. Kimura, M. Hirano, and H. Hosono, Phys. Status Solidi A **206**, 2187 (2009).

[17] H. Yabuta, N. Kaji, R. Hayashi, H. Kumomi, K. Nomura, T. Kamiya, M. Hirano, and H. Hosono, Appl. Phys. Lett. **97**, 072111 (2010).

[18] A. Bhatia, G. Hautier, T. Nilgianskul, A. Miglio, J. Sun, H. J. Kim, K. H. Kim, S. Chen, G.-M. Rignanese, X. Gonze, and J. Suntivich, Chem. Mater. **28**, 30 (2016).

[19] P. Shuk, H.-D. Wiemhöfer, U. Guth, W. Göpel, and M. Greenblatt, Solid State Ionics **89**, 179 (1996).

[20] A. Walsh, G. W. Watson, D. J. Payne, R. G. Edgell, J. Guo, P.-A. Glans, T. Learmonth, and K. E. Smith, Phys. Rev. B **73**, 235104 (2006).

[21] A. Matsumoto, Y. Koyama, and I. Tanaka, Phys. Rev. B **81**, 094117 (2010).

[22] P. Hohenberg and W. Kohn, Phys. Rev. **136**, B864 (1964).

[23] W. Kohn and L. J. Sham, Phys. Rev. **140**, A1133 (1965).

[24] J. Heyd and G. E. Scuseria, J. Chem. Phys. **120**, 7274 (2004).

[25] J. Heyd, G. E. Scuseria, and M. Ernzerhof, J. Chem. Phys. **124**, 219906 (2006).

[26] G. Kresse and J. Hafner, Phys. Rev. B **48**, 13115 (1993).

[27] G. Kresse and J. Furthmüller, Phys. Rev. B **54**, 11169 (1996).

[28] P. E. Blöchl, Phys. Rev. B **50**, 17953 (1994).

[29] G. Kresse and D. Joubert, Phys. Rev. B **59**, 1758 (1999).

[30] J. P. Perdew, A. Ruzsinszky, G. I. Csonka, O. A. Vydrov, G. E. Scuseria, L. A. Constantin, X. L. Zhou, and K. Burke, Phys. Rev. Lett. **100**, 136406 (2008).

[31] J. P. Perdew, Int. J. Quantum Chem. **28**, 497 (1985).

[32] M. Marezio, Acta Crystallogr. **20**, 723 (1966).

[33] A. Zunger, S.-H. Wei, L. G. Ferreira, and J. E. Bernard, Phys. Rev. Lett. **65**, 353 (1990).

[34] S.-H. Wei, L. G. Ferreira, J. E. Bernard, and A. Zunger, Phys. Rev. B **42**, 9622 (1990).

[35] H. Peelaers, D. Steiauf, J. B. Varley, A. Janotti, and C. G. Van de Walle, Phys. Rev. B **92**, 085206 (2015).

[36] M. Baldini, D. Gogova, K. Irmscher, M. Schmidbauer, G. Wagner, and R. Fornari, Cryst. Res. Technol. **49**, 552 (2014).

[37] F. Fuchs and F. Bechstedt, Phys. Rev. B **77**, 155107 (2008).

[38] L. F. J. Piper, A. DeMasi, S. W. Cho, K. E. Smith, F. Fuchs, F. Bechstedt, C. Körber, A. Klein, D. J. Payne, and R. G. Egdell, Appl. Phys. Lett. **94**, 022105 (2009).

[39] F. P. Sabino, L. N. Oliveira, S.-H. Wei, and J. L. F. Da Silva, J. Phys.: Condens. Matter **29**, 085501 (2017).

[40] H. G. Na, T.-K. Jung, J.-W. Lee, S.-K. Hyun, Y. J. Kwon, A. Mirzaei, T.-B. Kim, Y.-C. Shin, H.-J. Choi, H. W. Kim, and C. Jin, Mater. Res. Express **3**, 095016 (2016).